Multimedia Tools and Applications (2019) 78:27891–27914
https://doi.org/10.1007/s11042-019-7621-5

Improved homomorphic filtering using fractional derivatives for enhancement of low contrast and non-uniformly illuminated images

Kanwarpreet Kaur [1] • Neeru Jindal [1] • Kulbir Singh [1]

Received: 2 June 2018 / Revised: 31 January 2019 / Accepted: 8 April 2019 /
Published online: 28 June 2019

Abstract
The main objective of the image enhancement is to improve the visual appearance or quality of an image. In this paper, the proposed scheme aims to improve the performance of the homomorphic filtering by employing the fractional derivatives with Discrete Fourier Transform (DFT) and Fractional Fourier Transform (FrFT). FrFT in combination with fractional derivative provides two fractional orders as extra degrees of freedom, thus, providing more design flexibility. This paper uses Grunwald-Letnikov (GL) fractional derivative to enhance the high and mid frequency components non-linearly while preserving the low frequency components. In the proposed approach, modification of homomorphic filtering technique is done on the basis of fractional derivative and FrFT to enhance the low contrast and non-uniformly illuminated images. The effectiveness of the proposed work is evaluated on the basis of various image assessment parameters such as PSNR, information entropy, universal image quality index, etc. on several images of different sizes. The proposed scheme outperforms the existing state-of-the-art techniques by providing better image visual quality and image information in terms of average PSNR and entropy values. The improvement in the average PSNR and information entropy is in the range 0.2635–50.37 dB and 0.02–42% respectively for standard images as well as for images with different contrast and illumination conditions.

Keywords Homomorphic filtering · Fractional derivative · Fractional Fourier transform · Peak signal to noise ratio · Universal image quality index

✉ Kulbir Singh
ksingh@thapar.edu

Kanwarpreet Kaur
kkaur_phd16@thapar.edu

Neeru Jindal
neeru.jindal@thapar.edu

Extended author information available on the last page of the article

1 Introduction

In today's era, there is requirement of the image acquisition devices to capture the images for various practical applications ranging from medical to surveillance [11, 14]. But, sometimes captured images are not suitable for processing due to improper imaging conditions like non-uniform illumination, luminescence level etc. Since, illumination is crucial to improve the optimum image quality, so, there is need of enhancement for non-uniformly illuminated images.

Several image enhancement techniques exist to improve the quality of images in terms of both visual appearance and quantitative measures [1, 4, 13, 20, 35, 36, 50, 51]. These are further divided into the spatial and frequency domain techniques. In spatial domain techniques, the operation is performed directly on the pixels while in frequency domain techniques, the image is transformed into the frequency domain before applying any operation on the image [11, 14]. The transformation has been done using the Discrete Fourier Transform (DFT), Wavelet Transform (WT), Discrete Cosine Transform (DCT), Fractional Fourier Transform (FrFT), Discrete Fractional Cosine Transform (DFrCT), Linear Canonical Transform (LCT) etc. [2, 10, 11, 14, 15, 28, 33, 37]. There are various image enhancement techniques for low contrast and non-uniformly illuminated images such as Histogram Equalization (HE), Single Scale Retinex (SSR), Multi Scale Retinex (MSR), Homomorphic Filtering (HF), Linear Contrast Adjustment (LCA), Contrast Limited Adaptive Histogram Equalization (CLAHE) etc. [4, 11, 14, 50, 51]. Moreover, the issue of non-uniform illumination can be resolved by using the frequency domain technique such as Homomorphic Filtering (HF). In addition to image enhancement, it also sharpens the edges of the image. It is applied in various applications such as medical images, underwater images, face recognition etc. [1, 7, 13, 16, 19, 27, 29, 31, 35, 36, 45, 47].

Sheet et al. [35] modified the Brightness Preserving Dynamic Histogram Equalization (BPDHE) technique by computing the fuzzy histogram to perform smoothing before dividing the image into sub-histograms. It increases the ability of technique to preserve brightness and contrast enhancement with additional advantage of less computation time in comparison to BPDHE [13]. Median-Mean Based Sub-Image-Clipped Histogram Equalization (MMSICHE) preserves images. But, these methods can be used only for images with substantial peaks in the histogram. So, HF has been introduced for the enhancement of non-uniformly illuminated images. In [45], Tseng and Lee used image fusion in addition to the DCT based HF to combine the various enhanced images having different exposures to get the final output image. In [19], Lee and Tseng presented a DCT based matrix homomorphic filtering technique on the grayscale and color images.

Nowadays, image enhancement is mostly done with the fractional derivatives because they are able to enhance the low frequency details in smooth areas and sharpen the high frequency details. Thus, fractional derivatives have been used in various signal and image processing applications [3, 5, 8, 9, 12, 17, 18, 21, 30, 38, 39]. In [30], YiFeiPU−2 is considered to be better among the six fractional derivative masks and algorithms analyzed by Pu et al. for the texture enhancement on the basis of error analysis. Garg and Singh [9] improved GL based fractional differential operator for enhancing the textural information of an image that depends on the intensity factor and order of fractional operator. Besides, some recent works such as [40, 41] on image enhancement are based on Deep Neural Networks (DNNs). Actually, the image enhancement techniques based on fractional derivatives by using Deep Neural Network (DNN) is still not common in the existing literature. Moreover, the existing literature does not provide a comparison between DNN based image enhancement methods and fractional derivative based image enhancement methods. This may be due to the fact that the DNN approaches are designed for different scenarios. For instance, DNN methods are useful, when we need to deal with very large datasets with a large number of features and complex classification, thereby increasing the computation cost or execution time. Moreover, most of the existing recent image enhancement techniques such as [5, 12] are based on this concept. Therefore, in this paper, the proposed scheme is evaluated by considering most of the recent image enhancement methods based on fractional derivatives in order to make the comparison feasible.

In [19, 45] DCT has been used for the transformation of image into the frequency domain in HF. Although, DCT provides more accumulation of energy as compared to other transforms. But, it is unable to extract the local spectral features. In this paper, two techniques are presented for enhancement of the low contrast and non-uniformly illuminated images as well as sharpening of the edges. The first technique employs the fractional derivative (GL) instead of high pass filter while the second technique involves a combination of fractional derivative with FrFT to take the advantage of two extra degrees of freedom. FrFT is used instead of DCT in the proposed technique as its energy is also concentrated in the central region [24]. The performance of the proposed technique is evaluated and compared with other image enhancement techniques on the basis of various image assessment parameters [1, 11, 35, 36, 45]. The proposed scheme provides better image visual quality and image information in terms of average PSNR and entropy values.

The paper is organized as follows: Section 2 discussed about the preliminaries used in the paper. Section 3 depicts the proposed HF technique based on the fractional derivative as well as the combination of fractional derivative with FrFT. Section 4 discussed the simulated results of the proposed work and comparison with the existing techniques. The conclusion and future scope are presented in Section 5.

2 Preliminaries

2.1 Fractional derivative

Fractional Order Calculus (FOC) is a generalization of the integer order calculus. FOC has the capability to model systems more accurately in comparison to the integer orders. The commonly used fractional order derivatives are Riemann–Liouville (RL), Grünwald–Letnikov (GL), Caputo etc. Due to the discrete nature, GL derivative is used in most of the applications. The GL based derivative of a function $z(t)$ is given as [22, 23]:

$$ {}_cD_t^{\vartheta}\, z(t) = \lim_{h\to 0} \frac{1}{\Gamma(\vartheta)h^{\vartheta}} \sum_{k=0}^{\left(\frac{t-c}{h}\right)} \frac{\Gamma(\vartheta+k)}{\Gamma(k+1)} z(t-kh) \tag{1} $$

where, c and t are lower and upper limits of the integration. Here, ϑ ε R^+ (real numbers) such that $m-1<\vartheta<m$, where, m is the operation order (integer). Here, Γ(.) is the Euler's gamma function and h is the sampling period, where, $\left(\frac{t-c}{h}\right)$ is an integer and k ranges from 0 to $\left(\frac{t-c}{h}\right)$.

2.2 Fractional Fourier Transform (FrFT)

Fractional Fourier Transform (FrFT) is an important signal processing tool that rotates the signal in the time-frequency plane by an angle 'α' [33]. The FrFT of the signal $z(t)$ is given by [25, 26]:

$$ Z_{\alpha}(u_{\alpha}) = \int_{-\infty}^{\infty} z(t) K_{\alpha}(t, u_{\alpha}) dt \tag{2} $$

where, $0 < |a| < 2$, $\alpha = a\pi/2$ and $K_\alpha(t, u_\alpha)$ represents the Kernel function defined as:

$$K_\alpha(t, u_\alpha) = \begin{cases} \sqrt{\frac{1-i\cot\alpha}{2\pi}}\exp\left[i\left(\frac{t^2+{u_\alpha}^2}{2}\right)cot\ \alpha - i\,u_\alpha\,t\,csc\alpha\right] & if\ \alpha \neq n\pi \\ \delta(t-u) & if\ \alpha = 2n\pi \\ \delta(t+u) & if\ \ \alpha+\pi = 2n\pi \end{cases} \tag{3}$$

and $\delta(t)$ represents the Dirac's delta function. The signal is restored by taking the FrFT with the rotation angle of '-α', i.e., by replacing 'α' with '-α' in eq. (2) and (3). The two-dimensional FrFT is required to process the images in the frequency domain. The two-dimensional FrFT is taken separately in x and y directions. The separable two-dimensional FrFT has two orders α and β for x and y directions, i.e., $0 < \alpha < \pi/2$ and $0 < \beta < \pi/2$ is given below:

$$Z_{\alpha,\beta}(u_\alpha, v_\beta) = \int_{-\infty}^{\infty}\int_{-\infty}^{\infty} z(x,y) K_{\alpha,\beta}(x, y, u_\alpha, v_\beta)\,dx\,dy \tag{4}$$

where, α and β are the rotation angles.

The Kernel function $K_{\alpha,\beta}(x, y, u_\alpha, v_\beta)$ is defined as:

$$K_{\alpha,\beta}(x, y, u_\alpha, v_\beta) = K_\alpha(x, u_\alpha)\,K_\beta(y, v_\beta) \tag{5}$$

$$= \frac{1}{2\pi}\sqrt{1-i\cot\alpha}\sqrt{1-i\cot\beta}\,\exp\left[i\left(\frac{x^2+{u_\alpha}^2}{2}\right)cot\ \alpha - i\,u_\alpha x\csc\alpha\right]\exp\left[i\left(\frac{y^2+{v_\beta}^2}{2}\right)cot\beta - i\,v_\beta\,y\csc\beta\right] \tag{6}$$

The signal is restored by taking FrFT with the rotation angle of '-α' and '-β', that is, by replacing 'α' with '-α' and 'β' with '-β' in eq. (4)–(7). The proposed work uses two-dimensional Discrete Fractional Fourier Transform (2D-DFrFT) [26]. The (K, L)-point 2D-DFrFT is given as:

$$Z_{\alpha,\beta}(u_\alpha, v_\beta) = \sum_{y=0}^{L-1}\left[\sum_{x=0}^{K-1} z(x,y)\exp\left[i\left(\frac{x^2+{u_\alpha}^2}{2}\right)cot\ \alpha - i\,u_\alpha x\csc\alpha\right]\right]\exp\left[i\left(\frac{y^2+{v_\beta}^2}{2}\right)cot\beta - i\,v_\beta\,y\csc\beta\right] \tag{7}$$

The 2D-DFrFT for matrix $K \times L$ is determined by applying the one-dimensional DFrFT to each row of the matrix and afterwards to the column of the resultant.

2.3 Homomorphic Filtering

The HF technique is based on the illumination-reflectance model. Illumination refers to the amount of source illumination which is incident on the scene to be viewed denoted by (x, y). Reflectance refers to the amount of illumination that is reflected by the entities present in scene denoted by $R(x, y)$. Intensity of image (x, y) at spatial coordinates (x, y) is given by:

$$F(x, y) = I(x, y)R(x, y) \tag{8}$$

where, $0 < (x, y) < \infty$ and $0 < R(x, y) < 1$. The nature of illumination depends on the source of illumination while the reflectance depends on the attributes of the image entities. Reflectance is bounded by zero and one which means, total absorption and total reflectance, respectively. In this technique, the logarithm of the original image is taken, which maps the image from multiplicative domain into the additive domain. Image obtained after the logarithm operation is transformed into the frequency domain, after which the linear filtering is done that amplified the high frequencies while attenuating the low frequencies. Then, the enhanced image is obtained by taking the exponential of inverse transform of the image which is filtered also as shown in Fig. 1.

The HF method used the High Pass Filter (HPF) for the enhancement of image which is the procedure to capture the important properties such as geometry, reflectivity, and illumination. The basic ideal high pass filters are used in the modified form in this technique. This modification is done by including two parameters γ_L and γ_H in the equation of ideal high pass filter such that $\gamma_L < 1$ while, $\gamma_H > 1$ as shown in eq. (9):

$$\mathrm{H}(u,v) = (\gamma_H - \gamma_L)^*(HPF) + \gamma_L \tag{9}$$

Here, $\mathrm{H}(u, v)$ is modified equation for HPF in the frequency domain. The parameters γ_H and γ_L decreases the contribution made by low frequencies, whereas, increases the contribution made by the high frequencies. This technique increases the contrast of images as well as sharpens the edges of the images [11].

3 Proposed scheme

On the basis of HF technique [45], an improved HF technique is presented to achieve better visual quality and more information detail from the enhanced images. DCT transform [19, 45] provides accumulation of energy but it doesn't provide the local spectral features. The improved HF technique used fractional derivative and FrFT to enhance the high frequency features. In this paper, two techniques are proposed for enhancement of the low contrast and non-uniformly illuminated images. The first technique employs the fractional derivative (GL) instead of high pass filter while the second technique involves a combination of fractional derivative with FrFT to take the advantage of two extra degrees of freedom. The significance of the proposed algorithms is to achieve the enhancement of the low contrast and non-uniformly illuminated images as well as sharpening of the edges with the utilization of the fractional derivative and fractional derivative in combination with FrFT.

3.1 Proposed Algorithm 1: Fractional derivative based HF

In this algorithm, the fractional derivative is used to enhance the low contrast and non-uniformly illuminated images and sharpening the edges of image. The block diagram of the proposed algorithm based on fractional derivative is shown in Fig. 2.

In this technique, the logarithm of intensity as given in eq. (8) is taken before applying the transform because the transform of product of two functions is not separable.

$$\mathrm{z}(x,y) = \ln(\mathrm{F}(x,y)) = \ln(\mathrm{I}(x,y)) + \ln(\mathrm{R}(x,y)) \tag{10}$$

where, $z(x, y)$ is the logarithm of $\mathrm{F}(x, y)$.

$$Z(u,v) = \mathcal{T}\big(\mathrm{z}(x,y)\big) = \mathrm{F}_{\mathrm{I}}(u,v) + \mathrm{F}_{\mathrm{R}}(u,v) \tag{11}$$

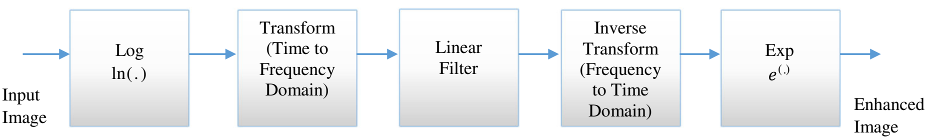

Fig. 1 Generalized homomorphic filtering technique [14]

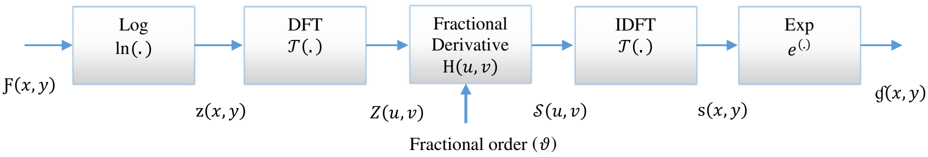

Fig. 2 Proposed HF technique based on fractional derivative

Here, $\mathcal{T}\big(z(x,y)\big)$ and $Z(u, v)$ refers to the DFT of $z(x, y)$. $Ƒ_Ɨ(u, v)$ and $Ƒ_{Ʀ}(u, v)$ is the DFT of $\ln(Ɨ(x, y))$ and $\ln(Ʀ(x, y))$ respectively. The GL fractional derivative is used for the analysis in DFT.

The precise form of the GL based fractional operator [30] is given by the following equation:

$$\frac{d^{\vartheta}}{dt^{\vartheta}}z(t)=\lim_{h\to 0}\frac{1}{\Gamma(-\vartheta)h^{\vartheta}}\sum_{k=0}^{(n-1)}\frac{\Gamma(k-\vartheta)}{\Gamma(k+1)}z\left(t+\frac{\vartheta h}{2}-kh\right) \tag{12}$$

The GL based fractional derivative is derived by inserting the values of signals on the non-nodes assuming $\vartheta = 0, \pm 2, \pm 4, \ldots$, considering the nodes at $z(t+h-kh)$, $z(t-kh)$ and $z(t-h-kh)$.

The interpolation is done using the Lagrange's 3-point interpolation method [9, 30]:

$$z(\tau)\cong\frac{(\tau-t+kh)(\tau-t+h+kh)}{2h^2}z(t+h-kh)-\frac{(\tau-t-h+kh)(\tau-t+h+kh)}{h^2}z(t-kh)$$
$$+\frac{(\tau-t+kh)(\tau-t-h+kh)}{2h^2}z(t-h-kh) \tag{13}$$

Let $\tau=\left(t+\frac{\vartheta h}{2}-kh\right)$ and interpolating it, the equation comes out to be:

$$z\left(t+\frac{\vartheta h}{2}-kh\right)\cong\left(\frac{\vartheta}{4}+\frac{\vartheta^2}{8}\right)z(t+h-kh)+\left(1-\frac{\vartheta^2}{4}\right)z(t-kh)+\left(-\frac{\vartheta}{4}+\frac{\vartheta^2}{8}\right)z(t-h-kh) \tag{14}$$

$$\frac{d^{\vartheta}}{dt^{\vartheta}}z(t)\cong\frac{1}{\Gamma(-\vartheta)h^{\vartheta}}\sum_{k=0}^{(n-1)}\frac{\Gamma(k-\vartheta)}{\Gamma(k+1)}\left[z_k+\frac{\vartheta}{4}(z_{k-1}-z_{k+1})+\frac{\vartheta^2}{8}(z_{k-1}-2z_k+z_{k+1})\right] \tag{15}$$

The coefficients of the filter obtained from eq. (15) are in the spatial domain. So, the DFT of the fractional derivative will be obtained in order to compute the frequency domain coefficients required in the HF technique. Then, the fractional derivative $\mathrm{H}(u, v)$ is applied on the obtained Fourier Transform coefficients.

$$\mathcal{S}(u,v)=\mathrm{H}(u,v)Z(u,v)=\mathrm{H}(u,v)\,Ƒ_Ɨ(u,v)+\mathrm{H}(u,v)\,Ƒ_{\mathrm{R}}(u,v) \tag{16}$$

where, $\mathcal{S}(u, v)$ is the DFT of the result obtained after filtering operation. The obtained coefficients after IDFT is given by:

$$\mathrm{s}(x,y)=\mathcal{T}^{-1}\big(\mathrm{H}(u,v)Z(u,v)\big)=\mathrm{s}(x,y)=Ɨ'(x,y)+Ʀ'(x,y) \tag{17}$$

where, $Ɨ'(x,y)=\mathcal{T}^{-1}(\mathrm{H}(u,v)\,Ƒ_Ɨ(u,v))$ and $Ʀ'(x,y)=\mathcal{T}^{-1}(\mathrm{H}(u,v)\,Ƒ_{\mathrm{R}}(u,v))$. The enhanced image obtained after the exponential operation is given by:

$$ɠ(x,y)=e^{\mathrm{s}(x,y)}=e^{Ɨ'(x,y)}e^{Ʀ'(x,y)}=Ɨ_0(x,y)Ʀ_0(x,y) \tag{18}$$

where, $Ɨ_0(x,y)=e^{Ɨ'(x,y)}$ and $Ʀ_0(x,y)=e^{Ʀ'(x,y)}$.

3.2 Proposed Algorithm 2: Fractional derivative FrFT based HF

In this technique, the fractional derivative is used in combination with DFrFT to enhance the edges of the low contrast and non-uniformly illuminated images. The DFrFT is applied in eq. (11) for transforming the image into frequency domain. This technique also uses GL fractional derivative as discussed in Algorithm 1. Instead of computing the DFT, DFrFT of eq. (15) will be obtained in order to compute the frequency domain coefficients required in the HF technique. Similarly, IDFrFT is used to obtain the spatial domain coefficients instead of IDFT. The block diagram of the proposed algorithm based on fractional derivative in combination with FrFT is shown in Fig. 3.

Pseudo code for the proposed scheme

Inputs: $\mathfrak{F}$, $\boldsymbol{\vartheta}$, $\boldsymbol{\alpha}$, $\boldsymbol{\beta}$
Output: $\mathbf{Z_o}$
$\mathfrak{F}$**: Test Image**
$\boldsymbol{\vartheta}$**: Order of derivative operator**
$\boldsymbol{\alpha}$, $\boldsymbol{\beta}$ **: Order of FrFT operator**
$\mathcal{T}$ **( ): Transform operator**
$\mathrm{H}(\,)$**: GL based fractional derivative operator**
start
$\mathrm{H}(x, y)$ =Compute the GL fractional operator using eq. (15);
$\mathrm{H}_{DFrFT}(u, v) = \mathcal{T}(\mathrm{H}(x, y), \alpha, \beta)$
$\mathrm{H}_{DFT}(u, v) = \mathcal{T}(\mathrm{H}(x, y))$
$\mathrm{z}(x, y) = \ln(\mathfrak{F}(x, y))$
$Z(u, v) = \mathcal{T}(\mathrm{z}(x, y))$
$\mathcal{S}(u, v) = \mathrm{H}(u, v) Z(u, v)$
$\mathrm{s}(x, y) = \mathcal{T}^{-1}(\mathcal{S}(u, v))$
$\mathfrak{g}(x, y) = e^{(\mathrm{s}(x,y))}$
end
Note: **For Algorithm 1,** $\mathrm{H}(u, v) = \mathrm{H}_{DFT}(u, v)$
For Algorithm 2, $\mathrm{H}(u, v) = \mathrm{H}_{DFrFT}(u, v)$

4 Experimental results

The adequacy of proposed techniques is confirmed using the MATLAB R2016a on a system with an Intel® CPU 2.7 GHz processor with 16 GB RAM. The effectiveness of the proposed scheme is also evaluated with different images. The comparison of the proposed algorithms is done with the existing techniques that is, HE [11], BDPFHE [35], MMSICHE [36], HF [1] and DCT based HF [45].

4.1 Performance analysis for images from standard datasets

In this section, the performance of proposed techniques is evaluated on various original images of different sizes from different datasets namely The USC-SIPI Image Database, TraitImage,

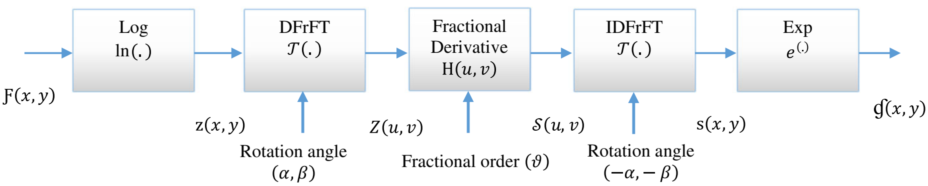

Fig. 3 Proposed HF technique based on the combination of fractional derivative and FrFT

Segmentation by Regions, Image Databases and in-built MATLAB images as shown in Fig. 4 [11, 34, 42, 43].

The enhanced images for the test images obtained using both Proposed Algorithm 1 and Algorithm 2 and existing techniques [1, 11, 35, 36, 45] are shown in Fig. 5. The performance of the enhancement of images is evaluated with the different performance metric parameters such as Peak Signal to Noise Ratio (PSNR), Mean Square Error (MSE), Information Entropy, Structural Similarity Index Measure (SSIM) and Universal Image Quality Index (UIQI).

The MSE formula is given by [32]:

$$MSE = \frac{1}{kl} \sum_{i=0}^{k-1} \sum_{j=0}^{l-1} [A(i,j) - O(i,j)]^2 \tag{19}$$

where, A and O are the images for comparison with size $k \times l$.

The PSNR is given by [32]:

$$PSNR = 10\ log_{10}\left(\frac{{Max_I}^2}{MSE}\right) \tag{20}$$

where, Max_I is the maximum value of a pixel.

Table 1 shows the Average PSNR for the different test images for various techniques. The optimal order of fractional derivative and transform order 'a' is mentioned in Table 1 that provides the best results. Maximum average PSNR is obtained for the proposed scheme for fractional derivative order of range 0.11–0.124 for transform order 0.99. It is interpreted that the enhanced images obtained with the fractional derivatives and DFrFT are more similar to the original images. Average PSNR is high for proposed scheme for all the considered images because the fractional derivatives enhance the high-frequency information present in the images. The amplitude and phase information of the image in DFrFT depends on its transform

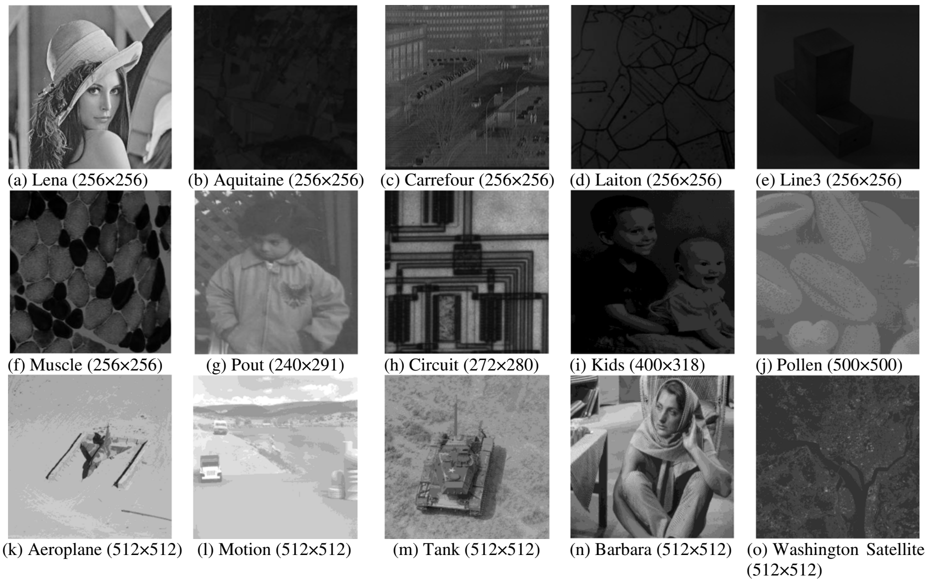

(a) Lena (256×256) (b) Aquitaine (256×256) (c) Carrefour (256×256) (d) Laiton (256×256) (e) Line3 (256×256)
(f) Muscle (256×256) (g) Pout (240×291) (h) Circuit (272×280) (i) Kids (400×318) (j) Pollen (500×500)
(k) Aeroplane (512×512) (l) Motion (512×512) (m) Tank (512×512) (n) Barbara (512×512) (o) Washington Satellite (512×512)

Fig. 4 Test images used for simulation of different sizes

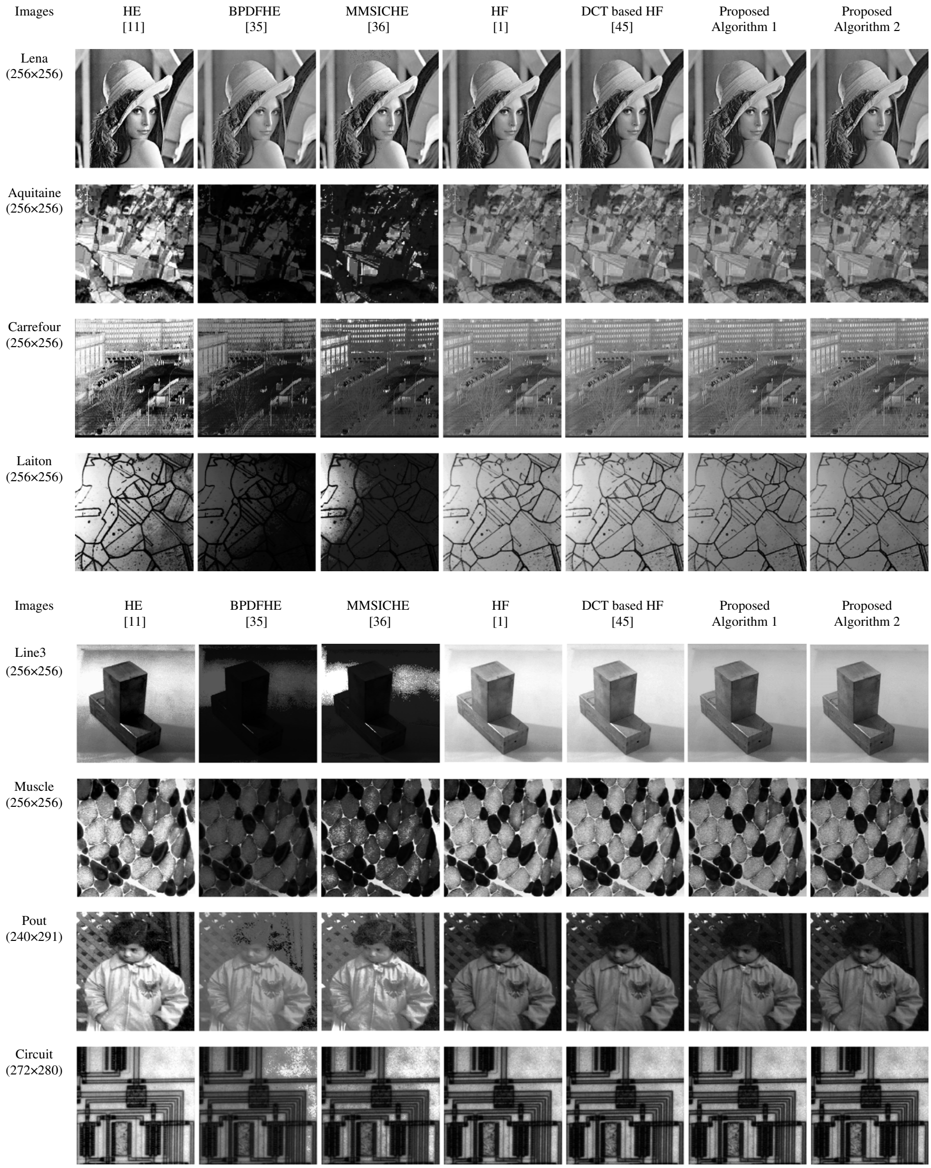

Fig. 5 Enhanced test images obtained with proposed algorithms in comparison to the existing techniques

order [24]. The results of PSNR in Algorithm 2 are better as DFrFT preserves the details of the texture of the image with an increase in transform order. Moreover, it is clear from the visual perception that the proposed scheme is better than the existing techniques [1, 11, 35, 36, 45] as shown in Fig. 5. The average PSNR obtained is maximum for Algorithm 2 as it exploited the advantage of both fractional derivative and DFrFT. From the eq. (19) and (20), it is clear that lesser the MSE, more the PSNR, better the quality of enhanced image. Table 2 shows the MSE of different test images for a proposed scheme in comparison to the existing techniques.

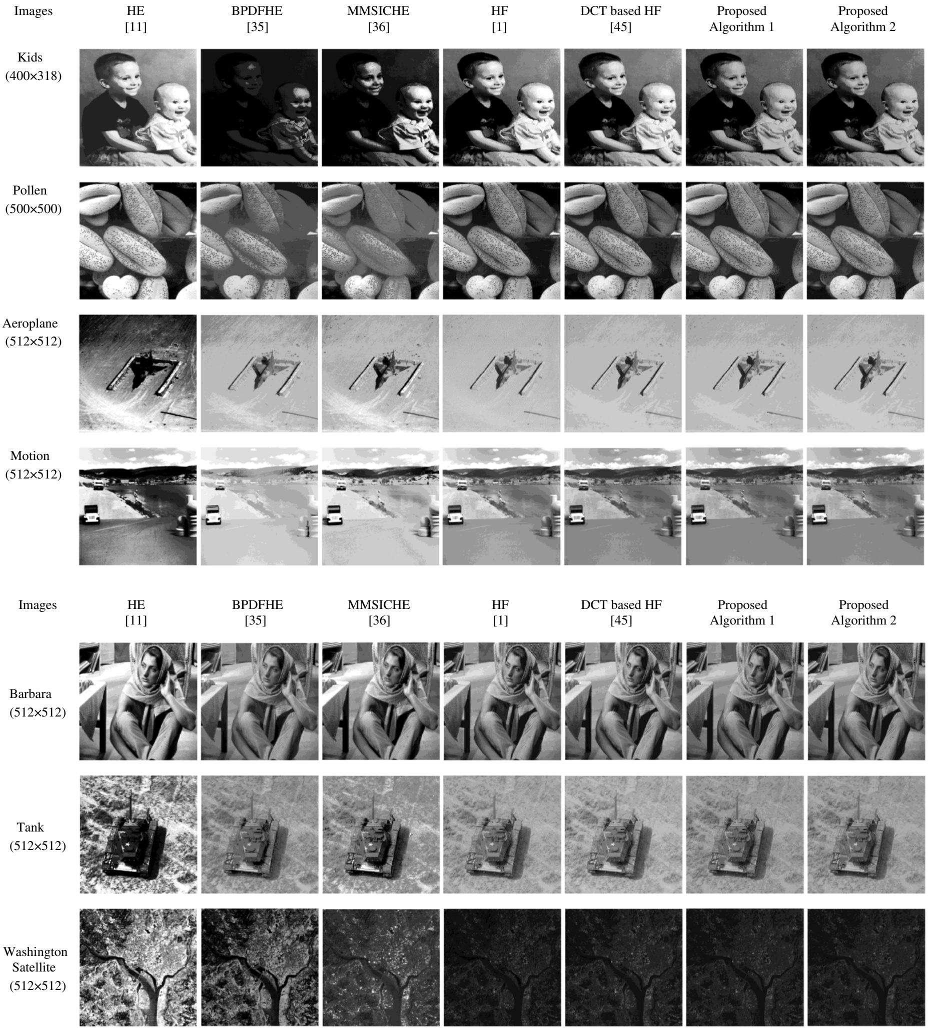

Fig. 5 (continued)

On the basis of Shannon's information, the entropy of an image is given by [44]:

$$E = -\sum_{i=0}^{255} P_i log_2 P_i \tag{21}$$

where, E is entropy, P_i is i's probability in the image. Table 3 shows the information entropy for the different test images for different techniques.

Information entropy of the proposed scheme is more as compared to the existing techniques [1, 11, 35, 36, 45] for all the considered images because it enhances the high frequency information while preserving low and medium frequency details. As observed from Table 3, Algorithm 2 provides more detailed information about the image. The information entropy for the images of Aquitaine and Line3 is almost comparable for both proposed algorithms.

Table 1 Average PSNR (dB) for the test images of different sizes

Image	a	ϑ (Alg.1)	ϑ (Alg.2)	HE [11]	BPDFHE [35]	MMSICHE [36]	HF [1]	DCT based HF [45]	Proposed Algorithm 1	Proposed Algorithm 2
Lena (256 × 256)	0.99	0.115	0.113	19.1126	32.0306	24.9145	30.3044	33.1415	36.6290	**36.6292**
Aquitaine (256 × 256)	0.99	0.124	0.12	6.0723	22.8354	15.7086	42.6306	43.9511	56.1616	**56.4412**
Carrefour (256 × 256)	0.99	0.12	0.12	9.3942	19.5349	18.3140	36.3847	36.7659	39.6785	**41.9095**
Laiton (256 × 256)	0.99	0.121	0.12	6.4105	22.5813	13.5690	42.4720	43.1712	48.4561	**48.4567**
Line3 (256 × 256)	0.99	0.124	0.121	6.0746	21.5813	11.8777	42.9946	53.6186	55.5564	**55.5599**
Muscle (256 × 256)	0.99	0.12	0.12	8.5072	26.8801	16.9935	38.2126	38.8858	40.0898	**41.0756**
Pout (240 × 291)	0.99	0.115	0.115	13.3148	25.1368	19.1888	31.8041	37.8613	40.9053	**47.1212**
Circuit (272 × 280)	0.99	0.115	0.115	12.6530	26.6781	20.0388	33.740	39.5597	40.3788	**41.6339**
Kids (400 × 318)	0.99	0.12	0.12	6.8236	22.8815	13.4034	41.5921	44.5675	45.3904	**46.0547**
Pollen (500 × 500)	0.99	0.11	0.11	11.7339	16.5445	16.5309	32.0538	38.5385	49.2873	**50.9277**
Aeroplane(512 × 512)	0.99	0.11	0.11	10.2277	27.4883	24.0326	27.8160	30.5231	40.2197	**42.8448**
Motion(512 × 512)	0.99	0.114	0.112	9.2512	23.2713	17.5430	26.8615	44.9075	46.2069	**47.3556**
Barbara (512 × 512)	0.99	0.115	0.114	18.0464	33.3304	24.3215	31.0498	33.2956	35.6999	**35.7668**
Tank (512 × 512)	0.99	0.115	0.115	13.7901	29.0108	22.0606	30.2198	31.9571	37.8322	**42.0287**
Washington Satellite (512 × 512)	0.99	0.12	0.11	9.2130	16.5394	21.9976	36.1327	37.0283	42.3851	**42.5879**

The bold values correspond to the highest value of PSNR (dB)

Table 2 MSE for the test images of different sizes

Images	HE [11]	BPDFHE [35]	MMSICHE [36]	HF [1]	DCT based HF [45]	Proposed Algorithm 1	Proposed Algorithm 2
Lena (256 × 256)	797.6729	40.7400	209.7148	60.6233	31.5447	14.1307	**14.1304**
Aquitaine (256 × 256)	16,064	338.4894	1746.7	3.5483	2.6180	0.1574	**0.1476**
Carrefour (256 × 256)	7475.9	723.7576	958.7034	14.9491	13.6927	7.0021	**4.1892**
Laiton (256 × 256)	14,860	358.8806	2858.8	3.6803	3.1330	0.9285	**0.9280**
Line3 (256 × 256)	16,056	451.5964	4220	3.2630	0.2826	0.1820	**0.1805**
Muscle (256 × 256)	9169.7	133.3723	1299.4	9.8135	8.4042	6.3694	**5.0760**
Pout (240 × 291)	3031.1	199.2492	783.7943	42.9209	10.6402	5.2790	**1.2617**
Circuit (272 × 280)	3530	139.7250	644.4671	27.4826	7.1963	5.9594	**4.4637**
Kids (400 × 318)	13,512	334.9111	2969.9	4.5068	2.2716	1.8795	**1.6129**
Pollen (500 × 500)	4362.1	1440.9	1445.4	40.5225	9.1039	0.7662	**0.5252**
Aeroplane (512 × 512)	6170.4	115.9455	256.9340	107.5186	57.6463	6.1818	**3.3776**
Motion (512 × 512)	7726.1	306.1593	1144.9	133.9448	2.1005	1.5574	**1.1954**
Barbara (512 × 512)	1019.6	30.2023	240.3974	51.0623	30.4454	17.5022	**17.2345**
Tank (512 × 512)	2716.9	81.6585	404.5918	61.8157	41.4351	10.7117	**4.0758**
Washington Satellite (512 × 512)	7794.4	1442.6	410.5071	15.8420	12.8900	3.7547	**3.5833**

The bold values correspond to the lowest value of MSE

The SSIM is represented by the given formula [49]:

$$SSIM(x,y)=\frac{\left(2\mu_x\mu_y+K_1\right)\left(2\sigma_{xy}+K_2\right)}{\left(\mu_x^2+\mu_y^2+K_1\right)\left(\sigma_x^2+\sigma_y^2+K_2\right)} \tag{22}$$

where,μ_x and μ_y represent the mean intensities, σ_x and σ_y represent the contrast while K_1 and K_2 represent the constants. Table 4 shows the SSIM for the different test images for various techniques.

SSIM value corresponds to the structural similarity between the original and reconstructed image. Enhancement of the low contrast and non-uniformly illuminated images results in the change in the structure of the image, thus reducing its SSIM. Although, SSIM of the proposed algorithms is less, but, it is still comparable to the existing techniques [1, 11, 35, 36, 45]. SSIM is high for Algorithm 1 in case of Aquitaine, Line3 and Motion as the change in structure is less after enhancement as compared to other techniques. It has kept the structure almost similar in addition to the enhancement of images. The Mean Structural Similarity Index Measure (SSIM) has also been calculated, but, it is observed that MSSIM is maximum for HF than the proposed techniques.

UIQI possess the ability to measure the structural distortion occurred during the process of degradation of an image. It indicates similarity and dissimilarity. It considers the three components for computing distortion while SSIM considers only one component, i.e., structure. In this, the comparison between two images is done by dividing it further into the three comparisons, that is, luminance $L(x, y)$, contrast $C(x, y)$ and structural comparison $S(x, y)$ given by [48]:

$$UIQI=L(x,y)\ C(x,y)\ S\ (x,y)=\frac{4\mu_x\mu_y\mu_{xy}}{\left(\mu_x^2+\mu_y^2\right)\left(\sigma_x^2+\sigma_y^2\right)} \tag{23}$$

Table 3 Information entropy for the test images of different sizes

Images	HE [11]	BPDFHE [35]	MMSICHE [36]	HF [1]	DCT based HF [45]	Proposed Algorithm 1	Proposed Algorithm 2
Lena (256 × 256)	5.9733	7.2328	7.4016	7.4429	7.3659	7.4625	**7.4673**
Aquitaine (256 × 256)	4.1892	3.8603	4.0986	4.2326	4.0070	**4.2098**	**4.2093**
Carrefour (256 × 256)	5.6752	5.8990	6.1364	6.2032	6.0778	6.1649	**6.1886**
Laiton (256 × 256)	4.6416	4.1345	4.6000	4.7792	4.5850	4.7476	**4.7689**
Line3 (256 × 256)	4.2204	3.7297	4.1374	4.2426	4.0781	**4.2135**	**4.2130**
Muscle (256 × 256)	5.8207	5.9309	6.3824	6.4072	6.3092	6.3731	**6.3940**
Pout (240 × 291)	5.4342	5.5950	5.7026	5.7551	5.9211	6.0630	**6.1032**
Circuit (272 × 280)	5.9358	6.8569	6.9134	6.9426	7.0745	7.1419	**7.1620**
Kids (400 × 318)	5.2508	5.0698	5.4609	5.4847	5.4728	5.4996	**5.5084**
Pollen (500 × 500)	4.9774	4.8087	4.9724	5.0339	5.0534	5.1878	**5.2472**
Aeroplane (512 × 512)	3.7451	3.9536	3.9914	4.0042	4.8442	5.1624	**5.3693**
Motion (512 × 512)	5.4164	5.8889	6.0083	5.9873	6.1608	6.1519	**6.1774**
Barbara (512 × 512)	5.9821	7.2688	7.4245	7.4680	7.3851	7.4768	**7.4910**
Tank (512 × 512)	4.9953	5.3276	5.7499	5.5017	6.2665	6.3892	**6.4181**
Washington Satellite (512 × 512)	2.8032	2.8500	2.8676	2.8688	4.2402	4.8377	**4.8433**

The bold values correspond to the highest value of Information Entropy

The $L(x, y)$, $C(x, y)$ and $S(x, y)$ is given by:

$$L(x,y) = \frac{2\mu_x\mu_y}{\mu_x^2 + \mu_y^2}$$
$$C(x,y) = \frac{2\sigma_x\sigma_y}{\sigma_x^2 + \sigma_y^2}$$
$$S(x,y) = \frac{2\sigma_{xy}}{\sigma_x + \sigma_y}$$

Table 4 SSIM for the test images of different sizes

Images	HE [11]	BPDFHE [35]	MMSICHE [36]	HF [1]	DCT based HF [45]	Proposed Algorithm 1	Proposed Algorithm 2
Lena (256 × 256)	0.8573	0.9616	0.9014	**0.9969**	0.9940	0.9881	**0.9869**
Aquitaine (256 × 256)	0.1296	0.4409	0.5820	0.9961	0.9956	**0.9983**	**0.9982**
Carrefour (256 × 256)	0.4012	0.6589	0.7616	**0.9970**	0.9918	0.9920	**0.9915**
Laiton (256 × 256)	0.1771	0.5953	0.7712	**0.9967**	0.9948	0.9941	**0.9939**
Line3 (256 × 256)	0.2562	0.5926	0.7536	0.9962	0.9981	**0.9985**	**0.9983**
Muscle (256 × 256)	0.3960	0.9463	0.7657	**0.9943**	0.9912	0.9882	**0.9878**
Pout (240 × 291)	0.5644	0.8281	0.6992	0.9972	**0.9977**	0.9955	**0.9945**
Circuit (272 × 280)	0.7445	0.9312	0.8825	0.9967	**0.9970**	0.9922	**0.9914**
Kids (400 × 318)	0.2146	0.8355	0.7332	**0.9750**	0.9734	0.9694	**0.9691**
Pollen (500 × 500)	0.4213	0.6128	0.6141	0.9974	**0.9992**	0.9965	**0.9951**
Aeroplane (512 × 512)	0.3140	0.7796	0.7188	0.9973	**0.9981**	0.9929	**0.9901**
Motion (512 × 512)	0.5355	0..9252	0.7985	0.9951	0.9971	**0.9974**	**0.9930**
Barbara (512 × 512)	0.8526	0.9649	0.9068	**0.9969**	0.9927	0.9885	**0.9871**
Tank (512 × 512)	0.4263	0.8643	0.6849	0.9969	**0.9978**	0.9896	**0.9879**
Washington Satellite (512 × 512)	0.2181	0.3722	0.7106	**0.9971**	0.9929	0.9900	**0.9917**

The bold values correspond to the highest value of SSIM where, μ_x and μ_y represent the mean intensities of original and distorted images, σ_x and σ_y represent the standard deviation of original and distorted images while σ_{xy} represent the covariance of both images. Table 5 shows the UIQI for different test images for various techniques.

It is almost comparable to other techniques, but as illustrated in Table 5, the Algorithm 2 has the highest UIQI for all considered test images of different sizes as compared to the existing techniques as well as the Algorithm 1. This may happen due to the use of DFrFT transform in combination with fractional derivatives because it enhances high frequency information as well as contrast while preserving the low and medium frequency details.

The effectiveness of the proposed techniques for the enhancement of the low contrast and non-uniformly illuminated images as well as strengthening of edges is demonstrated with the various image assessment parameters in Fig. 6. PSNR of the proposed techniques (Algorithm 2) is improved by 2.86–50.37 dB, thus, indicating that the images enhanced by proposed algorithms are of higher quality in comparison to existing algorithms [1, 11, 35, 36, 45] as shown in Fig. 6. The PSNR shows the improvement of 9.59 dB, 11.71 dB, 6.3 dB, and 3.4 dB in case of proposed techniques when compared to BPDFHE, MMSICHE, HF and DCT based HF for test image of Lena. MSE for HE and MMSICHE is not shown in Fig. 6 as it is large as compared to other techniques. Information Entropy shows the improvement of 0.3–20% when the comparison of proposed algorithm is done with the existing techniques for test image Lena [1, 11, 35, 36, 45]. Information entropy is improved by 3–42% with the Algorithm 2 for different images. The UIQI of all the images is close to one, indicating that even after enhancement the images are almost similar to original ones. Therefore, in Fig. 6, it is perceived that the proposed algorithms provide more enhancement and information details in comparison to the existing techniques [1, 11, 35, 36, 45]. The average time elapsed for execution of code ranges from 9.01 to 39.476 s for Algorithm 1 and 9.17 to 52.09 s for the Algorithm 2 for different images. The execution time varies in accordance with the number of pixels in the image.

Table 5 UIQI for the test images of different sizes

Images	HE [11]	BPDFHE [35]	MMSICHE [36]	HF [1]	DCT based HF [45]	Proposed Algorithm 1	Proposed Algorithm 2
Lena (256 × 256)	0.8872	0.9907	0.9524	0.9967	0.9986	0.9995	**0.9996**
Aquitaine (256 × 256)	0.2443	0.4264	0.7983	0.9852	0.9693	0.9947	**0.9998**
Carrefour (256 × 256)	0.6249	0.8043	0.9398	0.9964	0.9973	0.9988	**0.9995**
Laiton (256 × 256)	0.2265	0.4306	0.8540	0.9945	0.9948	0.9997	**0.9999**
Line3 (256 × 256)	0.1214	0.3216	0.8178	0.9872	0.9701	0.9704	**0.9957**
Muscle (256 × 256)	0.3027	0.9241	0.9488	0.9813	0.9845	0.9827	**0.9850**
Pout (240 × 291)	0.7804	0.9776	0.9149	0.9968	0.9992	0.9997	**0.9999**
Circuit (272 × 280)	0.7557	0.9910	0.8848	0.9944	0.9985	**0.9982**	**0.9982**
Kids (400 × 318)	0.1154	0.6520	0.7282	0.8617	0.8567	0.8354	**0.8698**
Pollen (500 × 500)	0.7301	0.8899	0.8754	0.9968	0.9992	0.9992	**0.9993**
Aeroplane (512 × 512)	0.7044	0.9958	0.9823	0.9967	0.9981	0.9991	**0.9993**
Motion (512 × 512)	0.6772	0.9843	0.9393	0.9967	0.9995	0.9996	**0.9999**
Barbara (512 × 512)	0.7914	0.7588	0.9309	0.9967	0.9987	0.9996	**0.9997**
Tank (512 × 512)	0.7874	0.9852	0.9539	0.9968	0.9978	0.9996	**0.9999**
Washington Satellite (512 × 512)	0.6489	0.9896	0.9689	0.9965	0.9971	0.9987	**0.9989**

The bold values correspond to the highest value of UIQI

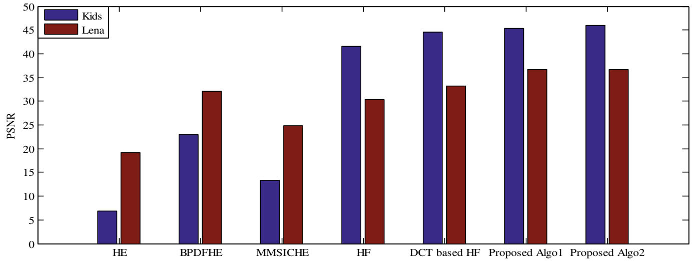

(a) PSNR

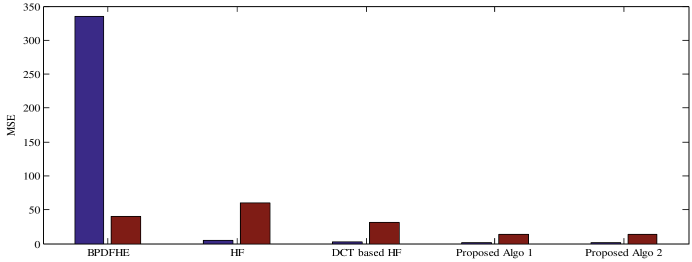

(b) MSE

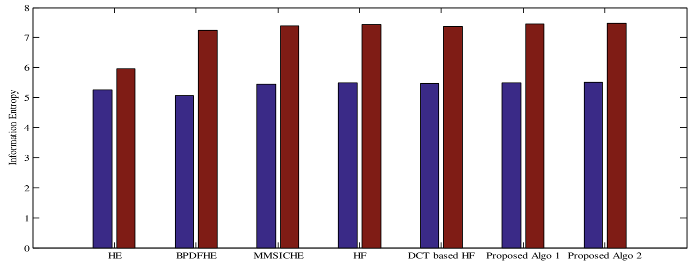

(c) Information Entropy

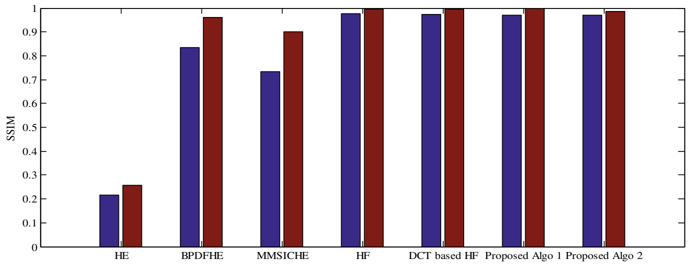

(d) SSIM

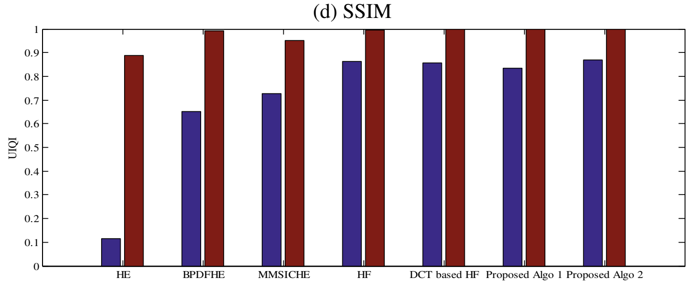

(e) UIQI

Fig. 6 Comparison of various image enhancement techniques on the basis of image assessment parameters for Kids and Lena Image

4.2 Performance analysis for images with different contrast and illumination conditions

In this section, the performance of proposed techniques is analyzed on datasets [6, 46] containing test images with different contrast and illumination conditions as shown in Fig. 7.

It is difficult to add all the images due to the space constraint. So, the enhanced images for some test images with different contrast and illumination conditions are shown in Fig. 8. It is clearly perceived from Fig. 8 that proposed algorithm results in more clarity in the enhanced images in comparison to the existing techniques. Tables 6, 7, 8, 9 and 10 depicts various performance parameters for different contrast and illumination conditions of various test images of different sizes.

It is worth noting that in the case of lossy compression such as JPEG, the PSNR value is constrained to 50 dB [20]. However, the PSNR value of greater than 50 dB is achieved in the case of proposed scheme because the test images (from datasets [11, 34, 42, 43]) used to evaluate the proposed scheme are in lossless file format. Secondly, this may also happen because the proposed scheme is based on fractional derivatives that results in the enhancement of high and mid frequency components non-linearly while preserving the low frequency components.

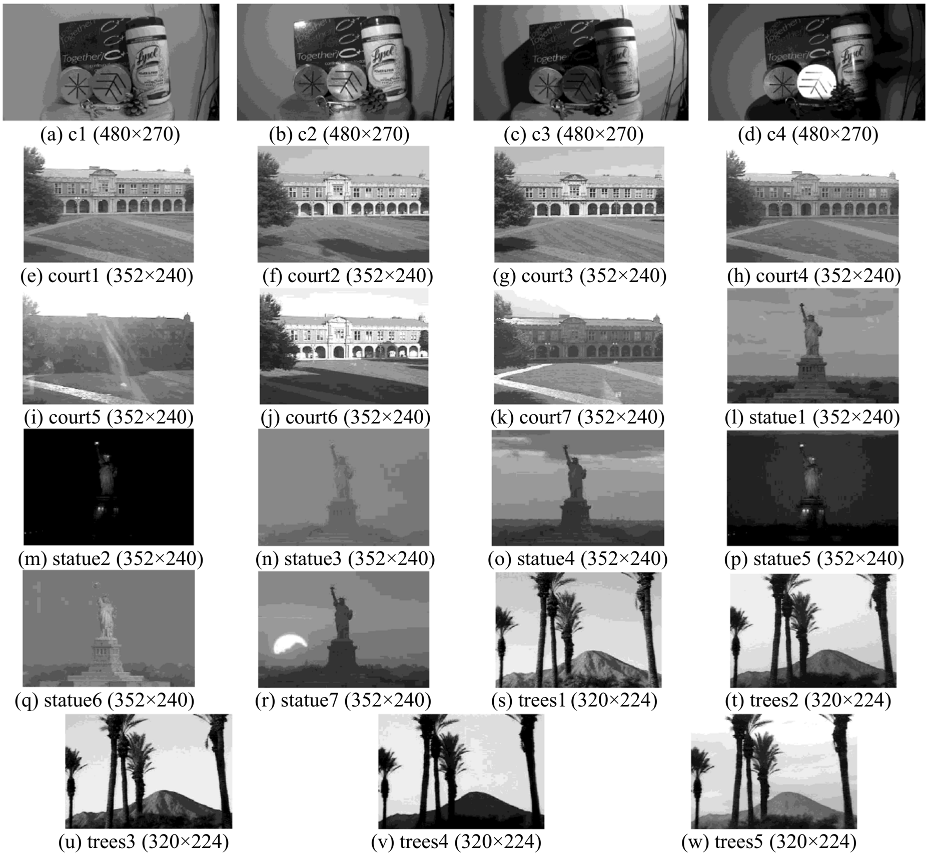

(a) c1 (480×270) (b) c2 (480×270) (c) c3 (480×270) (d) c4 (480×270)
(e) court1 (352×240) (f) court2 (352×240) (g) court3 (352×240) (h) court4 (352×240)
(i) court5 (352×240) (j) court6 (352×240) (k) court7 (352×240) (l) statue1 (352×240)
(m) statue2 (352×240) (n) statue3 (352×240) (o) statue4 (352×240) (p) statue5 (352×240)
(q) statue6 (352×240) (r) statue7 (352×240) (s) trees1 (320×224) (t) trees2 (320×224)
(u) trees3 (320×224) (v) trees4 (320×224) (w) trees5 (320×224)

Fig. 7 Test images with different contrast and illumination conditions

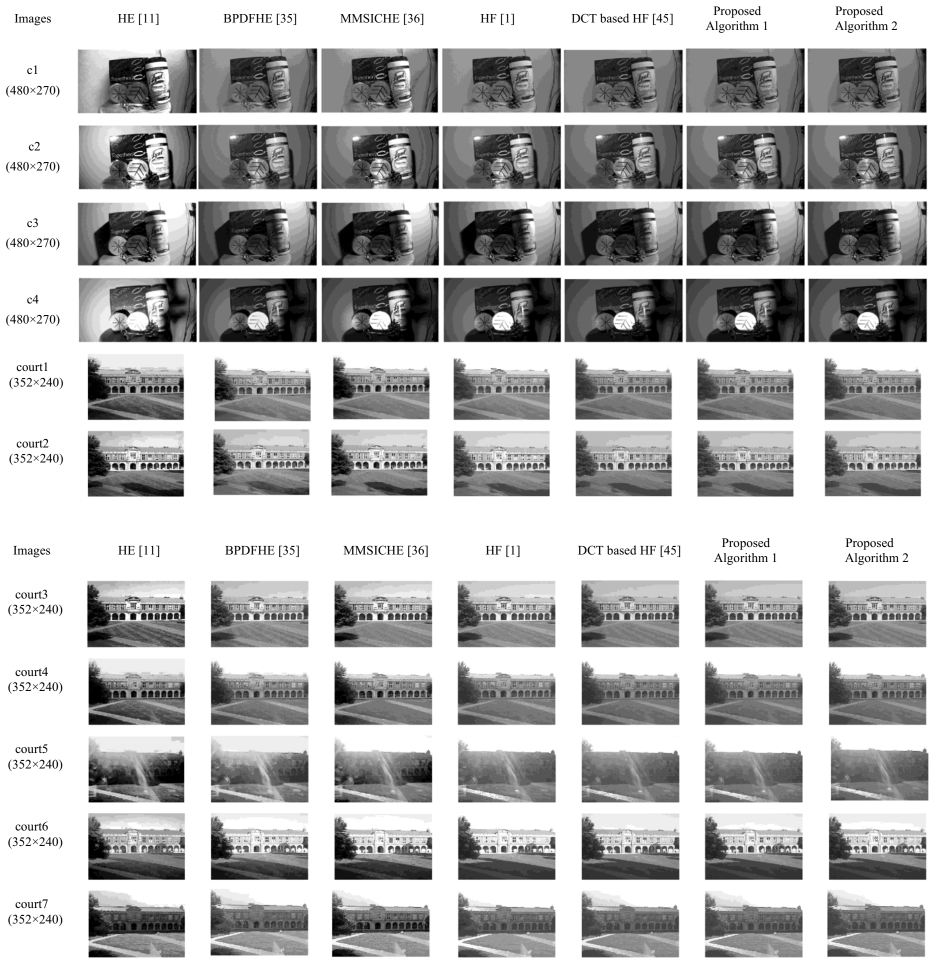

Fig. 8 Enhanced test images for different contrast and illumination conditions obtained with proposed algorithms in comparison to the existing techniques

Nevertheless, in order to confirm the above mentioned fact, the proposed scheme is further evaluated by considering the dataset images [46] in the JPEG file format. It is observed from Table 6 that maximum PSNR value achieved for the proposed scheme is of value 49.5650 dB (i.e. statue5 image) because the considered images are in JPEG file format. The PSNR value greater than 50 dB is achieved for lossless images such as TIFF, PNG file formats as shown in Table 1. It is also noted from Tables 6 to 10 that Algorithm 1 and Algorithm 2 provides high PSNR, information entropy, and UIQI in comparison to existing techniques even in the case of different contrast and illumination conditions for the same scene. The improvement in PSNR is 0.2635–42.2162 dB for Algorithm 1 and 0.2777–42.2273 dB for Algorithm 2 in case of images with different contrast and illumination conditions for the same scene. Furthermore, the improvement in information entropy is 0.02–32.63% for Algorithm 1 and 0.04–32.65% for Algorithm 2. It provides less SSIM but still it is comparable to existing techniques. Thus, the

Table 6 PSNR (dB) of test images of different sizes for different contrast and illumination conditions

Images	a	ϑ (Alg.1)	ϑ (Alg.2)	HE [11]	BPDFHE [35]	MMSICHE [36]	HF [1]	DCT based HF [45]	Proposed Algorithm 1	Proposed Algorithm 2
c1 (480 × 270)	0.99	0.101	0.102	15.3114	32.5079	24.0440	31.5845	36.2300	37.0236	**38.0061**
c2 (480 × 270)	0.99	0.1	0.1	14.7936	40.6294	26.2086	32.2338	36.6625	41.2364	**42.0412**
c3 (480 × 270)	0.99	0.1	0.099	16.1063	42.1522	29.0113	31.9091	36.5196	44.1992	**44.7229**
c4 (480 × 270)	0.99	0.11	0.1	11.0772	33.2892	25.2176	35.5958	38.1458	39.0281	**42.4131**
court1 (352 × 240)	0.99	0.1	0.101	17.5277	29.4207	25.3019	31.4187	31.9496	33.5973	**35.6522**
court2 (352 × 240)	0.99	0.099	0.1	19.1627	28.4535	24.8885	29.1546	32.3095	34.8946	**36.4592**
court3 (352 × 240)	0.99	0.11	0.089	17.8250	33.0481	26.3421	28.9811	32.0538	34.5488	**36.1930**
court4 (352 × 240)	0.99	0.1	0.101	18.2132	29.1301	24.4094	32.0264	32.4093	33.8759	**35.9653**
court5 (352 × 240)	0.99	0.101	0.1	16.5130	22.9681	22.8521	31.8055	32.3603	33.7766	**35.9038**
court6 (352 × 240)	0.99	0.099	0.095	19.3167	26.9741	25.8857	29.6506	30.8136	33.1486	**35.5446**
court7 (352 × 240)	0.99	0.1	0.1	17.9846	32.2216	22.4249	30.4675	32.0868	33.7396	**34.6735**
statue1 (352 × 240)	0.99	0.099	0.1	14.8999	18.2137	20.3881	30.7429	35.9935	37.4618	**38.4567**
statue2 (352 × 240)	0.99	0.09	0.085	5.2102	29.7716	31.4098	46.6751	47.1598	47.4264	**47.4375**
statue3 (352 × 240)	0.99	0.1	0.099	11.8799	25.5291	17.1101	31.0501	36.5901	38.9595	**39.1175**
statue4 (352 × 240)	0.99	0.1	0.1	16.1122	24.1622	21.5810	30.8668	36.2873	37.4857	**38.6202**
statue5 (352 × 240)	0.99	0.102	0.098	7.6403	29.4486	20.1157	39.3951	48.5631	48.9179	**49.5650**
statue6 (352 × 240)	0.99	0.1	0.088	11.8494	17.3103	21.1218	31.3052	36.6349	37.1160	**37.8638**
statue7 (352 × 240)	0.99	0.101	0.1	14.9966	29.4654	22.1456	31.3305	36.7648	37.0283	**37.2220**
trees1 (320 × 224)	0.99	0.1	0.096	17.8756	31.4446	25.4135	28.2122	31.9663	37.7373	**38.4657**
trees2 (320 × 224)	0.99	0.099	0.089	16.4547	24.2129	25.3534	27.8049	31.5739	38.3925	**38.9549**
trees3 (320 × 224)	0.99	0.1	0.09	16.0068	30.3532	24.6174	27.7716	31.2206	36.9637	**37.8613**
trees4 (320 × 224)	0.99	0.1	0.084	15.3767	25.4795	22.9581	28.0353	31.8519	37.7928	**38.8509**
trees5 (320 × 224)	0.99	0.099	0.089	17.0289	32.1291	27.6434	28.8721	31.5028	37.9209	**38.8179**

The bold values correspond to the highest value of PSNR (dB)

Table 7 MSE of test images of different sizes for different contrast and illumination conditions

Images	HE [11]	BPDFHE [35]	MMSICHE [36]	HF [1]	DCT based HF [45]	Proposed Algorithm 1	Proposed Algorithm 2
c1 (480 × 270)	1914	36.4994	256.2613	45.1471	15.4911	12.9038	**10.2913**
c2 (480 × 270)	2156.3	5.6252	155.6757	38.8780	14.0225	4.8915	**4.0640**
c3 (480 × 270)	1593.8	3.9615	81.6480	41.8959	14.4919	2.4727	**2.1918**
c4 (480 × 270)	5074.1	30.4905	195.5778	17.9267	9.9655	8.1334	**3.7305**
court1 (352 × 240)	1149	74.3033	191.8195	46.9037	41.5065	28.4018	**17.6953**
court2 (352 × 240)	788.52	92.8400	210.9727	78.9982	38.2059	21.0680	**14.6946**
court3 (352 × 240)	1073	32.2307	150.9638	82.2178	40.5225	22.8139	**15.6235**
court4 (352 × 240)	977.13	79.4463	235.5831	40.7790	37.3375	26.6371	**16.4647**
court5 (352 × 240)	1451.4	328.3027	337.1849	42.9074	37.7620	27.2535	**16.6993**
court6 (352 × 240)	761.03	130.5180	167.6906	70.4729	53.9168	31.4938	**21.9789**
court7 (352 × 240)	1034.2	38.9866	372.0399	58.3891	40.2158	27.4867	**22.1680**
statue1 (352 × 240)	2104.2	981.0873	594.6642	54.8014	16.3580	11.6655	**9.2771**
statue2 (352 × 240)	19,591	68.5356	47.0005	1.3982	1.2506	1.1761	**1.1074**
statue3 (352 × 240)	4217.8	182.0420	1264.9	51.0593	14.2584	8.2629	**7.9676**
statue4 (352 × 240)	1591.7	249.3818	451.8313	53.2601	15.2881	11.6015	**8.9342**
statue5 (352 × 240)	11,196	73.8271	633.1578	7.4744	0.9053	0.8342	**0.7188**
statue6 (352 × 240)	4247.5	1208	502.2224	48.1464	14.1121	12.6324	**10.6342**
statue7 (352 × 240)	2057.9	73.5431	396.7531	47.8661	13.6961	12.8899	**12.3277**
trees1 (320 × 224)	1060.5	46.6253	186.9521	98.1432	41.3472	10.9484	**9.2579**
trees2 (320 × 224)	1471	246.4861	189.5579	107.7928	45.2572	9.4152	**8.2716**
trees3 (320 × 224)	1630.8	59.9462	224.5624	108.6227	49.0929	13.0831	**10.6401**
trees4 (320 × 224)	1885.4	184.1333	329.0556	102.2241	42.4515	10.8094	**8.4722**
trees5 (320 × 224)	1288.8	39.8259	111.8768	84.3090	46.0041	10.4951	**8.5367**

The bold values correspond to the lowest value of MSE

Table 8 Information Entropy of test images of different sizes for different contrast and illumination conditions

Images	HE [11]	BPDFHE [35]	MMSICHE [36]	HF [1]	DCT based HF [45]	Proposed Algorithm 1	Proposed Algorithm 2
c1 (480 × 270)	5.7839	6.5291	6.7968	6.8654	6.8028	6.8718	**6.8770**
c2 (480 × 270)	5.9517	6.9986	7.2077	7.2756	7.2217	7.2849	**7.2872**
c3 (480 × 270)	5.9807	7.4473	7.6049	7.6498	7.6049	7.6641	**7.6681**
c4 (480 × 270)	5.9420	6.7627	7.0232	7.0297	7.0427	7.0509	**7.0789**
court1 (352 × 240)	5.2882	6.3159	6.4893	6.3712	6.5213	6.5487	**6.5533**
court2 (352 × 240)	5.8039	6.9490	7.1010	7.1436	7.1392	7.1788	**7.1872**
court3 (352 × 240)	5.9274	6.9920	7.2345	7.3020	7.2709	7.3083	**7.3178**
court4 (352 × 240)	5.2440	6.1570	6.3056	6.2052	6.3398	6.3629	**6.3706**
court5 (352 × 240)	5.2787	6.0049	6.1750	5.9927	6.2178	6.2231	**6.2335**
court6 (352 × 240)	5.8406	6.7430	6.9657	6.2622	7.0912	7.1236	**7.1264**
court7 (352 × 240)	5.6477	6.7338	6.8632	6.5830	6.9341	6.9493	**6.9573**
statue1 (352 × 240)	5.1384	5.5909	5.7574	5.8164	5.8071	5.8175	**5.8273**
statue2 (352 × 240)	2.9151	2.4790	2.3821	3.1585	3.1501	3.1594	**3.1598**
statue3 (352 × 240)	3.2699	3.3373	3.4963	3.5080	3.4960	3.5042	**3.5053**
statue4 (352 × 240)	5.7295	6.2640	6.3534	6.4021	6.4020	6.4062	**6.4214**
statue5 (352 × 240)	4.9074	5.0970	5.2634	5.3797	5.3927	5.3950	**5.3960**
statue6 (352 × 240)	3.5425	3.8720	4.0504	4.0710	4.0876	4.0938	**4.2852**
statue7 (352 × 240)	5.3904	5.7740	6.0225	6.0395	6.0725	6.0754	**6.0888**
trees1 (320 × 224)	5.9524	7.1295	7.2620	7.3575	7.3212	7.3595	**7.3624**
trees2 (320 × 224)	5.7584	6.6547	6.8175	6.8909	6.8539	6.8988	**6.8995**
trees3 (320 × 224)	5.6859	6.6162	6.7609	6.8472	6.7956	6.8567	**6.8586**
trees4 (320 × 224)	5.2492	5.9042	6.0505	6.1203	6.0653	6.1229	**6.1270**
trees5 (320 × 224)	5.9093	7.1738	7.2012	6.8693	7.3417	7.3833	**7.3866**

The bold values correspond to the highest value of Information Entropy

Table 9 SSIM of test images of different sizes for different contrast and illumination conditions

Images	HE [11]	BPDFHE [35]	MMSICHE [36]	HF [1]	DCT based HF [45]	Proposed Algorithm 1	Proposed Algorithm 2
c1 (480 × 270)	0.7958	0.9736	0.9055	**0.9974**	0.9957	0.9965	**0.9962**
c2 (480 × 270)	0.8323	0.9897	0.9381	**0.9973**	0.9959	0.9958	**0.9967**
c3 (480 × 270)	0.8804	0.9949	0.9599	0.9967	0.9965	**0.9968**	**0.9966**
c4 (480 × 270)	0.6813	0.9880	0.9547	**0.9964**	0.9961	0.9963	**0.9962**
court1 (352 × 240)	0.7900	0.9479	0.9218	0.9959	0.9940	**0.9976**	**0.9975**
court2 (352 × 240)	0.8413	0.9427	0.9100	0.9971	0.9936	**0.9973**	**0.9972**
court3 (352 × 240)	0.8014	0.9633	0.9268	**0.9971**	0.9930	0.9968	**0.9969**
court4 (352 × 240)	0.7615	0.9456	0.9038	0.9962	0.9944	**0.9979**	**0.9976**
court5 (352 × 240)	0.7300	0.8944	0.8671	0.9963	0.9961	**0.9979**	**0.9977**
court6 (352 × 240)	0.8352	0.9223	0.9061	0.9949	0.9930	**0.9968**	**0.9967**
court7 (352 × 240)	0.8039	0.9548	0.8303	0.9955	0.9939	**0.9973**	**0.9972**
statue1 (352 × 240)	0.6518	0.7622	0.7249	0.9977	0.9975	**0.9988**	**0.9984**
statue2 (352 × 240)	0.0263	0.8515	0.9217	**0.9724**	**0.9724**	0.9723	**0.9722**
statue3 (352 × 240)	0.6375	0.8838	0.8010	0.9980	0.9990	**0.9994**	**0.9993**
statue4 (352 × 240)	0.8080	0.8884	0.8550	0.9977	0.9980	**0.9988**	**0.9986**
statue5 (352 × 240)	0.4061	0.9032	0.9177	0.9952	0.9959	**0.9963**	**0.9963**
statue6 (352 × 240)	0.6331	0.8002	0.8867	0.9981	0.9981	**0.9989**	**0.9981**
statue7 (352 × 240)	0.7746	0.9255	0.8554	0.9974	0.9984	**0.9988**	**0.9986**
trees1 (320 × 224)	0.8758	0.9712	0.9255	**0.9972**	0.9950	0.9959	**0.9957**
trees2 (320 × 224)	0.7733	0.9010	0.9048	**0.9972**	0.9956	0.9967	**0.9965**
trees3 (320 × 224)	0.7991	0.9605	0.9215	**0.9971**	0.9944	0.9955	**0.9952**
trees4 (320 × 224)	0.5877	0.8726	0.8953	**0.9961**	0.9953	0.9956	**0.9956**
trees5 (320 × 224)	0.8555	0.9620	0.9334	0.9901	0.9961	**0.9971**	**0.9967**

The bold values correspond to the highest value of SSIM

Table 10 UIQI of test images of different sizes for different contrast and illumination conditions

Images	HE [11]	BPDFHE [35]	MMSICHE [36]	HF [1]	DCT based HF [45]	Proposed Algorithm 1	Proposed Algorithm 2
a c1 (480 × 270)	0.8852	0.9961	0.9745	0.9965	0.9989	0.9991	**0.9994**
c2 (480 × 270)	0.8567	0.9988	0.9659	0.9966	0.9989	0.9995	**0.9997**
c3 (480 × 270)	0.8592	0.9938	0.9407	0.9953	0.9991	**0.9992**	**0.9992**
c4 (480 × 270)	0.5618	0.9892	0.9850	0.9944	0.9975	0.9978	**0.9979**
court1 (352 × 240)	0.8332	0.9831	0.9502	0.9975	0.9989	0.9992	**0.9995**
court2 (352 × 240)	0.8553	0.9789	0.9504	0.9968	0.9989	0.9993	**0.9996**
court3 (352 × 240)	0.8384	0.9972	0.9663	0.9967	0.9989	0.9993	**0.9996**
court4 (352 × 240)	0.8476	0.9938	0.9454	0.9975	0.9990	0.9993	**0.9995**
court5 (352 × 240)	0.8193	0.9833	0.9468	0.9975	0.9989	0.9992	**0.9996**
court6 (352 × 240)	0.8969	0.9575	0.9389	0.9972	0.9989	0.9993	**0.9997**
court7 (352 × 240)	0.8357	0.9955	0.9224	0.9973	0.9989	0.9992	**0.9994**
statue1 (352 × 240)	0.8175	0.9364	0.9195	0.9967	0.9991	0.9994	**0.9995**
statue2 (352 × 240)	0.0167	0.6076	0.7818	0.9547	0.9520	**0.9525**	**0.9525**
statue3 (352 × 240)	0.7334	0.9820	0.8956	0.9968	0.9990	0.9994	**0.9995**
statue4 (352 × 240)	0.8440	0.9667	0.9172	0.9968	0.9992	0.9994	**0.9995**
statue5 (352 × 240)	0.3228	0.9181	0.9666	0.9918	0.9935	**0.9919**	**0.9919**
statue6 (352 × 240)	0.7417	0.9164	0.9473	0.9969	0.9991	0.9991	**0.9993**
statue7 (352 × 240)	0.8277	0.9774	0.9172	0.9968	0.9992	0.9992	**0.9993**
trees1 (320 × 224)	0.9023	0.9989	0.9818	0.9958	0.9967	**0.9995**	**0.9995**
trees2 (320 × 224)	0.9132	0.9651	0.9490	0.9960	0.9989	**0.9996**	**0.9996**
trees3 (320 × 224)	0.9437	0.9925	0.9957	0.9950	0.9981	0.9974	**0.9996**
trees4 (320 × 224)	0.7429	0.9081	0.9868	0.9938	0.9958	0.9971	**0.9973**
trees5 (320 × 224)	0.9147	0.9755	0.9791	0.9965	0.9990	0.9997	**0.9998**

The bold values correspond to the highest value of UIQI analysis done on the basis of different contrast and illumination conditions for the same scene confirms the efficacy of the proposed algorithms.

5 Conclusion

In this paper, two techniques based on fractional derivative and FrFT have been implemented. These techniques sharpened the edges of the image as well as enhanced the low contrast and non-uniformly illuminated images. The improvement in average PSNR of 2.86–20.49 dB has been obtained for the test images on comparison with the HF and DCT based HF. While, for HE, BPDFHE and MMSICHE improvement in PSNR is 2.44–50.37 dB for the different test images. The improvement of about 3–42% has been achieved in the information entropy for proposed techniques when compared with the HE, HF, and DCT based HF techniques. In the case of images with different contrast and illumination conditions for the same scene, the improvement in PSNR is 0.2635–42.2273 dB while for information entropy is 0.02–32.65% for the proposed algorithms. The analysis of proposed techniques on basis of various image assessment parameters shows more enhancement in comparison to the existing techniques. Thus, it has been observed that techniques based on fractional derivative and FrFT outperform the existing techniques. The future work involves the use of fractional derivative operators and FrFT for more image processing applications. Moreover, the future work will be devoted to perform the comparative analysis of fractional derivative based enhancement methods with DNN based image enhancement methods, which would further confirm the capability of the proposed technique.

References

1. Adelmann HG (1998) Butterworth equations for homomorphic filtering of images. Comput Biol Med 28(2): 169–181
2. Agarwal H, Atrey PK, Raman B (2015) Image watermarking in real oriented wavelet transform domain. Multimed Tools Appl 74(23):10883–10921
3. Almeida LB (1994) The fractional Fourier transform and time–frequency representation. IEEE Trans Signal Process 42(11):3084–3091
4. Bourne R (2010) Contrast Adjustment. In: Fundamentals of digital imaging in medicine. Springer, London, pp 109–135
5. Chen S, Zhao F (2018) The adaptive fractional order differential model for image enhancement based on segmentation. Int J Patt Recogn Artif Intell 32(3):184005
6. Chwyl B, Chung AG, Li FY, Wong A, Clausi DA (2015) Tiger: A texture-illumination guided energy response model for illumination robust local saliency. Proc IEEE Int Conf on Image Process (ICIP):1970–1974
7. Faraji MR, Qi X (2014) Face recognition under varying illumination based on adaptive homomorphic eight local directional patterns. IET Comput Vis 9(3):390–399
8. Gao C, Zhou J, Liu C, Pu Q (2015) Image enhancement based on fractional directional derivative. Int J Mach Learn Cyber 6(1):35–41
9. Garg V, Singh K (2012) An improved Grunwald-Letnikov Fractional Differential Mask for Image Texture Enhancement. Int J Adv Comput Sci Appl 3(3):130–135
10. Goel N, Singh K, Saxena R, Singh AK (2016) Multiplicative filtering in the linear canonical transform domain. IET Signal Process 10(2):173–181
11. Gonzalez RC, Woods RE (2008) Digital image processing. Prentice-Hall, NJ
12. Guan J, Ou J, Lai Z, Lai Y (2018) Medical image enhancement method based on the fractional order derivative and the directional derivative. Int J Patt Recogn Artif Intell 32(3):1857001
13. Ibrahim H, Kong NSP (2007) Brightness preserving dynamic histogram equalization for image contrast enhancement. IEEE Trans Consum Electron 53(4):1752–1758
14. Jain AK (1989) Fundamentals of digital image processing. Prentice-Hall, NJ

15. Jindal N, Singh K (2014) Image and video processing using discrete fractional transforms. Signal Image Video Process 8(8):1543–1553
16. Karamizadeh S, Abdullah SM, Cheraghi SM, Zamani M (2015) Filtering based illumination normalization techniques for face recognition. TELKOMNIKA Indonesian J Elect Eng Comput Sci 13(4):314–320
17. Kumar S, Singh K, Saxena R (2013) Closed-form analytical expression of fractional order differentiation in fractional Fourier transform domain. Circ Syst Sign Process 32(4):1875–1889
18. Kumar S, Saxena R, Singh K (2017) Fractional Fourier Transform and Fractional-Order Calculus-Based Image Edge Detection. Circuits Syst. Signal Process. 36(4):1493–1513
19. Lee SL, Tseng CC (2016) Image enhancement using DCT-based matrix homomorphic filtering method. Proc IEEE Asia Pacific Conf on Circuits and Systems (APCCAS): 1–4
20. Lin LH, Chen TJ (2018) Mutual Information Correlation with Human Vision in Medical Image Compression. Curr Med Imaging Rev 14(1):64–70
21. Lingaswamy S, Kumar D (2018) An efficient moving object detection and tracking system based on fractional derivative. Multimed Tools Appl: 1–19
22. Oldham KB, Spanier J (1974) The fractional calculus: theory and applications of differentiation and integration to arbitrary order. Academic, New York
23. Ortigueira MD (2011) Fractional calculus for scientists and engineers. Springer
24. Ozaktas HM, Zalevsky Z, Kutay MA (2001) The fractional fourier transform with applications in optics and signal processing. Wiley, New York
25. Pei SC, Ding JJ (2000) Closed-form discrete fractional and affine Fourier transforms. IEEE Trans Signal Process 48(5):1338–1353
26. Pei SC, Yeh MH (1998) Two dimensional discrete fractional Fourier transform. Signal Process 67(1):99–108
27. Prabhakar CJ, Kumar PU (2012) An image based technique for enhancement of underwater images. Int J Mach Intell 3(4):217–224
28. Proakis J, Manolakis D (2013) Digital signal processing: Principles, algorithms and applications. Pearson, India
29. Pu T, Wang S (2017) A perceptually motivated enhancement method for non-uniformly illuminated images. IET Comput Vis 12(4):424–433
30. Pu YF, Zhou JL, Yuan X (2010) Fractional Differential Mask: A Fractional Differential-Based Approach for Multiscale Texture Enhancement. IEEE Trans Image Process 19(2):491–511
31. Ramaraj M, Raghavan S, Khan WA (2013) Homomorphic filtering techniques for WCE image enhancement. Proc IEEE Int Conf Comput Intell Comput Res (ICCIC): 1–5
32. Richardson IEG (2003) H.264 and MPEG-4 video compression: Video coding for next-generation multimedia. Wiley, UK
33. Saxena R, Singh K (2005) Fractional Fourier transform: A novel tool for signal processing. J Indian Inst Sci 85(1):11–26
34. Segmentation by regions [Online] (2017) Available: http://www.tsi.enst.fr/pages/enseignement/ressources/mti/Seg.html
35. Sheet D, Garud H, Suveer A, Mahadevappa M, Chatterjee J (2010) Brightness preserving dynamic fuzzy histogram equalization. IEEE Trans Consum Electron 56(4):2475–2480
36. Singh K, Kapoor R (2014) Image enhancement via median-mean based sub-image-clipped histogram equalization. Optik 125(17):4646–4651
37. Singh G, Singh K (2018) Forensics for partially double compressed doctored JPEG images. Multimed Tools Appl 77(1):485–502
38. Singh K, Saxena R, Kumar S (2013) Caputo-based fractional derivative in fractional Fourier transform domain. IEEE J Emerg Sel Topics Circuits Syst 3(3):330–337
39. Suman S, Jha RK (2017) A new technique for image enhancement using digital fractional-order Savitzky–Golay differentiator. Multidim Syst Sign Process 28(2):709–733
40. Tao L, Zhu C, Xiang G, Li Y, Jia H, Xie X (2017) LLCNN: A convolutional neural network for low-light image enhancement. Proc IEEE Conf Visual Comm Image Process. (VCIP): 1–4
41. Tao L, Zhu C, Song J, Lu T, Jia H, Xie X (2017) Low-light image enhancement using CNN and bright channel prior. Proc IEEE Int Conf Image Process (ICIP): 3215–3219
42. The USC-SIPI Image Database [Online] (2017) Available: http://sipi.usc.edu/database/database.php
43. TraitImage [Online] (2017) Available: http://www.crm.umontreal.ca/~physnum/Ard/intro.html
44. Tsai DY, Lee Y, Matsuyama E (2008) Information entropy measure for evaluation of image quality. J Digital Imaging 21(3):338–347
45. Tseng CC, Lee SL (2017) A weak-illumination image enhancement method using homomorphic filter and image fusion. Proc 6th IEEE Global Conf. on Consumer Electronics (GCCE): 1–2
46. VIP Illumination Saliency Dataset [Online] (2019) Available: https://uwaterloo.ca/vision-image-processing-lab
47. Vishwakarma AK, Mishra A, Gaurav K, Katariya A (2012) Illumination reduction for low contrast color image enhancement with homomorphic filtering technique. Proc IEEE Int Conf Commun Syst Netw Technol (CSNT): 171–173

48. Wang Z, Bovik AC (2002) A universal image quality index. IEEE Signal Process Lett 9(3):81–84
49. Wang Z, Bovik AC, Sheikh HR, Simoncelli EP (2004) Image quality assessment: from error visibility to structural similarity. IEEE Trans Image Process 13(4):600–612
50. Zhou S, Zhang F, Siddique MA (2015) Range limited peak-separate fuzzy histogram equalization for image contrast enhancement. Multimed Tools Appl 74(17):6827–6847
51. Zuiderveld K (1994) Contrast limited adaptive histogram equalization. In: Heckbert PS (ed) Graphics Gems IV. Academic Press, UK, pp 474–485

Kanwarpreet Kaur received B. Tech degree in Electronics and Communication Engineering from Guru Nanak Dev Engineering College, Ludhiana in 2014. She received M. Tech degree in Electronics and Communication Engineering from Guru Nanak Dev Engineering College, Ludhiana in 2016. She is currently pursuing the Ph.D. degree in Electronics and Communication Engineering Department at Thapar Institute of Engineering and Technology, Patiala. Her research interests include signal processing and fractional calculus.

Neeru Jindal received the B.Tech. and M.Tech. degree in Electronics and Communication in 2002 and 2007 respectively from Punjab Technical University, Jalandhar, Punjab, India. She has received Ph.D. degree in 2014 from the Department of Electronics and Communication Engineering, Thapar Institute of Engineering and Technology, Patiala, Punjab, India. She has been involved in various research activities in the area of image and video processing. She holds the position of Assistant Professor in the department of Electronics and Communication Engineering, Thapar Institute of Engineering and Technology, Patiala, Punjab, India.

Kulbir Singh received the B.Tech. degree in 1997 from Punjab Technical University, Jalandhar, Punjab, India. He has received M.Tech. degree in 2000 and Ph.D. degree in 2006 from Thapar Institute of Engineering and Technology, Patiala, Punjab, India. He is having more than nineteen years of experience in research and academic activities. He has published more than 70 research papers in national and international journals/conference proceedings. He is a recipient of the Best Paper Award of the IETE Journal of Education for the year 2008. His research interests include Fractional Transforms, Signal Processing and Image Forensics. Presently he holds the position of Professor in Department of Electronics and Communication Engineering, Thapar Institute of Engineering and Technology, Patiala, Punjab, India.

Affiliations

Kanwarpreet Kaur [1] • **Neeru Jindal** [1] • **Kulbir Singh** [1]

[1] Department of Electronics and Communication Engineering, Thapar Institute of Engineering and Technology, Patiala, Punjab, India